Perceptual cycles travel across retinotopic space

Camille Fakche[1] and Laura Dugué[1,2]

[1] Université Paris Cité, CNRS, Integrative Neuroscience and Cognition Center, F-75006 Paris, France

[2] Institut Universitaire de France (IUF), Paris, France

Corresponding Author:

Camille Fakche

camille.fakche@gmail.com

Acknowledgements

This project has received funding from the European Research Council (ERC) under the European Union's Horizon 2020 research and innovation program (grant agreement No 852139 – Laura Dugué) and the Agence Nationale de la Recherche (ANR) - Deutsche Forschungsgemeinschaft (DFG) program (grant agreement No J18P08ANR00 – Laura Dugué). We also thank Kirsten Petras, Andrea Alamia, Rufin VanRullen and Frédéric Chavane for their useful comments on the manuscript.

Summary

Visual perception waxes and wanes periodically as a function of the phase of low-frequency brain oscillations (theta, 4-7 Hz; alpha, 8-13 Hz) [1-9]. Perceptual cycles are defined as the corresponding periodic modulation of perceptual performance (review [10, 11]). Here, using psychophysics, we tested the hypothesis that brain oscillations travel across the visual cortex, leading to predictable perceptual consequences across the visual field, i.e., perceptual cycles travel across the retinotopic visual space. An oscillating disk (inducer) was presented in the periphery of the visual field to induce brain oscillations at low frequencies (4, 6, 8 or 10 Hz) at a specific retinotopic cortical location. Target stimuli at threshold (50% detection) were displayed at random times during the periodic disk stimulation, at one of three possible distances from the disk. Electroencephalography (EEG) was recorded while participants performed a detection task. EEG analyses showed that the periodic stimulation produced a complex brain oscillation composed of the induced frequency and its first harmonic likely due to the overlap of the periodic response and the neural response to individual stimuli. This complex oscillation, which originated from a precise retinotopic position, modulated detection performance periodically at each target position and at each frequency. Critically, the optimal behavioral phase, i.e., of highest performance, of the 8 Hz and 10 Hz oscillations (alpha range) consistently shifted across target distance to the inducer. Together, the results demonstrate that alpha-induced perceptual cycles traveled across the retinotopic space in human observers at a propagation speed between 0.2 and 0.4 m/s.

Results

Studies suggest that the phase of low-frequency brain oscillations accounts for <20% of the trial-by-trial variability in behavioral performance [1, 4-6, 8, 12, 13]. We hypothesize that if brain oscillations are the support of visual perception, they should explain a larger portion of the variance observed in empirical data. We propose that not only the temporal aspect of brain signals but also their spatial organization must be jointly considered when investigating their

functional role. Invasive studies in mammals reveal that low-frequency oscillatory activity propagates within individual visual areas (V1, V2, V4, MT) with a phase shift between the source of the neural activity and more distal retinotopic positions [14-24]. In humans, although a few invasive studies in patients showed that low-frequency oscillations can propagate within individual non-visual brain areas [25-27], there is no electro-physiological study to date investigating the propagation of low-frequency oscillations in individual visual areas. This may be due to several methodological constraints including, for invasive studies, the usual lack of intracranial coverage over the visual system, and for non-invasive studies, the poor spatial resolution of magnetoencephalography (MEG) and EEG. The aim of the present study is to circumvent these issues. We build on [28] and use a well-established psychophysics approach combined with EEG and eye-tracking, to assess the propagation of brain oscillations across the visual cortex, leading to predictable perceptual consequences across the visual field, i.e., perceptual cycles travel across the retinotopic space.

Participants (n=15) performed a threshold visual detection task, while a luminance oscillating disk was concurrently presented in the periphery (eccentricity: 7.5°) to induce theta/alpha brain oscillations (4, 6, 8 and 10 Hz; EEG simultaneously recorded). Near-threshold target stimuli appeared at one of three possible eccentricities between a central fixation cross and the disk (**Figure 1A**; adjusted according to cortical magnification so each target measured 0.8 mm of diameter and were placed 0.8 mm away from each other in the cortex; see **Figure 1B**). We tested whether (1) the periodic disk stimulation modulates detection performance periodically at each target position, (2) the optimal phase (of highest performance) shifts as a function of distance from the disk suggesting that perceptual cycles travel across space (**Figure 1C**), and (3) the occurrence of such traveling properties depends on the induced frequency.

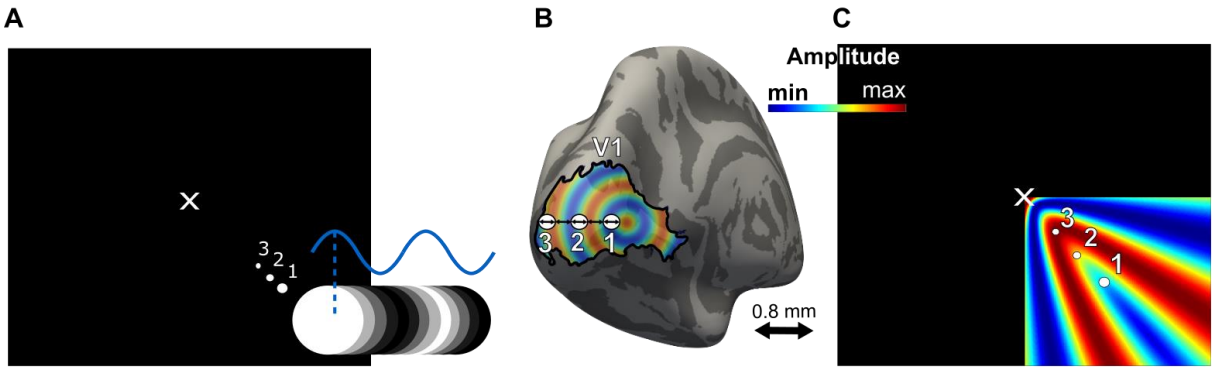

Figure 1. Experimental protocol. A. *A luminance oscillating disk (inducer) was presented in the periphery to induce brain oscillations in the visual cortex (e.g., V1). Participants were instructed to detect visual targets at threshold (50% detection) at three different positions in the retinotopic space, based on cortical magnification. Disks oscillated for a 30-seconds period during which 6 to 18 targets were presented at random times according to a decreasing probability distribution. Participants pressed the space bar when they detected the target (1-s response window after target onset)* ***B.*** *In the visual cortex, visual targets measured 0.8 mm of diameter and were placed 0.8 mm away from each other.* ***C.*** *Hypothesis: the oscillating disk, presented in the lower right corner, induced a brain oscillation that traveled across the retinotopic space (note that we concentrate our predictions to the quadrant in which the disk is presented). At an instant t, position 3 is located at the optimal phase of the oscillation (leading to the highest performance; i.e., max Amplitude), while position 1 is located at the non-optimal phase (i.e., min Amplitude).*

EEG activity was analyzed using frequency decomposition (Fast Fourier Transform, FFT, performed on the time series of each participant and electrode) and Event-Related Potentials (ERPs) measures to ensure that we successfully induced brain oscillations and to characterize the shape of the evoked response. First, peaks in the spectrum (as measured per SNR, averaged across participants and electrodes) were identified for each induced frequency (4, 6, 8 and 10 Hz; SNR > 1.43) and their first harmonics (8, 12, 16 and 20 Hz; SNR > 1.56), with topographies showing brain activity in the occipital cortex (for simplicity, frequencies were rounded to a whole number; real values are displayed in **Figure 2 left side of each panel**). Second, ERP analyses showed that the evoked signal is a complex oscillation composed of the induced frequency and its first harmonic (**Figure 2 right side of each panel**). We further

computed an FFT on the ERPs of electrode Oz. Peaks were again identified for each induced frequency (4, 6, 8 and 10 Hz; SNR > 2.52) and their first harmonics (8, 12, 16 and 20 Hz; SNR > 4.31; data not shown). These complex evoked responses were interpreted as the overlap between the periodic brain response (i.e., inducer) and the neural population response to individual stimuli (i.e., contrast change) at low frequencies, or alternatively, to the nonlinear nature of the visual system, i.e., nonlinear systems produce complex output consisting of the input frequency and multiple harmonics [29, 30]. Together, the EEG analyses confirm that we successfully induced theta/alpha oscillations in the visual cortex and show that the evoked signal is a complex oscillation composed of the induced frequency and its first harmonic [29, 30].

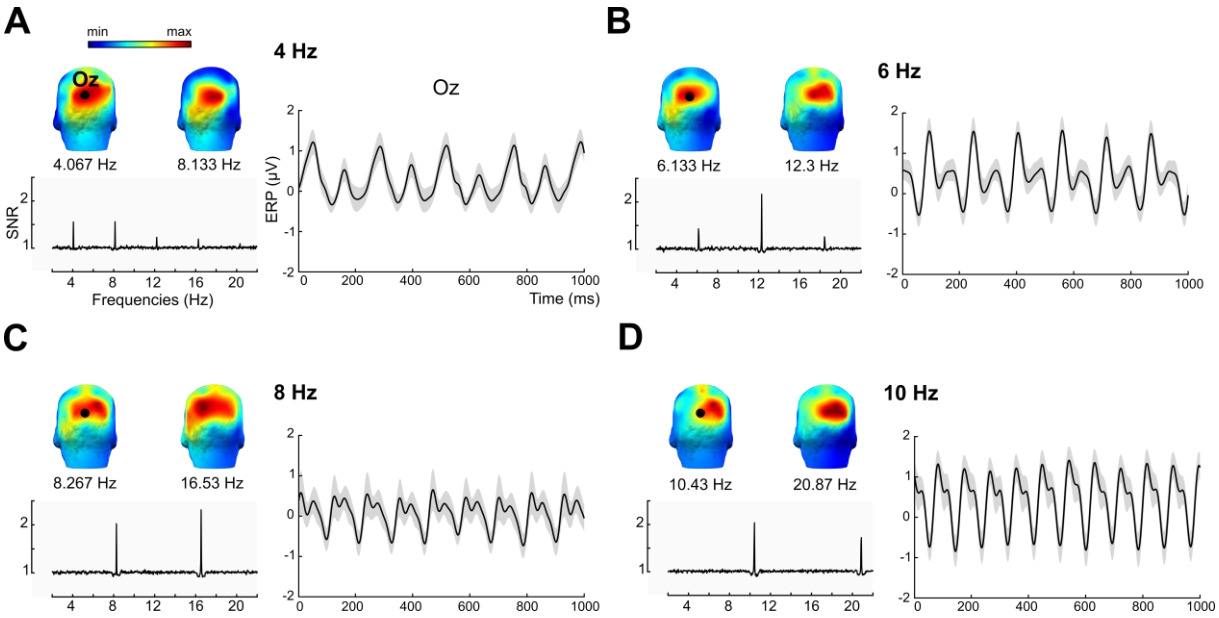

Figure 2. The oscillating disk evokes complex brain oscillations in the occipital cortex. *Left side of each panel, Fast Fourier Transform analyses performed on the EEG time series. Right side of each panel, ERP analyses, for induced frequencies of* ***A.*** *4,* ***B.*** *6,* ***C.*** *8 and* ***D.*** *10 Hz (rounded frequency values). Signal-to-noise ratio (SNR) amplitude averaged across 15 participants and all 62 electrodes, from 2 to 22 Hz. In each panel, a peak in SNR is identified for the induced frequency and its first harmonic. Topographies of the two SNR peaks revealed that we successfully induced brain oscillations in the visual cortex. Black dot, Electrode Oz. ERP of the Oz electrode computed on one-second epochs (the first-second epoch was removed to each 30-seconds blocks to avoid the EEG transient evoked response; each block*

represented 29 1-second epochs) averaged across participants (n=15). Solid black line, averaged ERP. Shaded area, standard error of the mean.

Second, we investigated whether detection performance was modulated periodically for each induced frequency and each target position. Targets (from 6 to 18 targets per 30 seconds-blocks) can appear at random delays during the periodic disk stimulation (from 1s to 29s from disk onset). Targets were binned according to the phase of the oscillating disk (7 bins/cycle; least number of bins to sample one oscillatory period while allowing a large number of trials per bin to achieve high statistical power). In each bin, detection performance was computed as per hit rate (correct target detection) for each participant, frequency, and target position. Finally, the data were averaged across participants and, given the complex shape of the ERP (**Figure 2**), fit to a complex sine function, separately for each frequency and target position (see **STAR Methods**). Detection performance showed a significant oscillatory pattern for each target position and frequency (Monte Carlo, Bonferroni corrected across frequencies and positions, p-value threshold < 0.01, corresponding to a Z-score threshold of 2.64, and a Cohen's d threshold of 1.86; **Figure 3**), and a clear optimal phase (of highest performance). The inducer modulated detection performance periodically, at each target position and at each frequency, with an average amplitude modulation (optimal to non-optimal hit rate difference) of 44.8 ± 3.4 %. A complementary analysis showed that behavioral performance was better explained when taking into account the spatial position of the targets. Specifically, we compared the amplitude modulation when detection performance was calculated disregarding target position, with the amplitude modulation calculated independently for each target position and then averaged across positions (two-tailed t-tests Bonferroni corrected for multiple comparisons: 4 Hz, p-value < 0.01, Cohen's d = -0.36, CI = [-0.05; -0.02]; 6 Hz, p-value < 0.01, Cohen's d = -0.28, CI = [-0.04; -0.01]; 8 Hz, p-value < 0.01, Cohen's d = -0.30, CI = [-0.04, -0.01]; 10 Hz, p-value < 0.01, Cohen's d = -0.58, CI = [-0.05; -0.03]). The amplitude modulation was significantly stronger when calculated position-by-position, suggesting that taking into account the spatial position of visual targets better explain perceptual performance.

Critically, we tested whether (1) perceptual cycles propagate across the retinotopic space, and (2) the occurrence of such traveling properties depends on the induced frequency. Propagation is defined as a shift in the optimal phase between two positions. To assess whether the optimal phase shifted as a function of target position, we computed the phase-locking values of the optimal phase (i.e., phase concentration of the distribution of optimal phases obtained with a bootstrap procedure; see **STAR Methods**) for each participant, target position, and frequency. A linear mixed effects model was implemented with frequency (4, 6, 8, 10 Hz), target position (1, 2, 3) and their interaction as fixed effects. Participant's intercepts and slopes for the effect of frequency and target position were considered random effects. The effects of frequency ($t(176) = 0.01$, p-value = 0.99, estimate ± standard error < 0.01 ± 0.01) and target position were not significant ($t(176) = 1.36$, p-value = 0.17, estimate = 0.02 ± 0.01). The interaction between frequency and target position was, however, significant ($t(176) = -0.01$, p-value = 0.05, estimate = -0.01 ± 0.01). Post-hoc analyses on the optimal phase difference (see **STAR Methods**; reported in degrees for easier readability of **Figure 3**) between each pair of target position (1 and 3, 1 and 2, and 2 and 3; Monte Carlo, FDR corrected across frequencies and positions, p-value threshold of 0.01, corresponding to Z-score threshold of 2.24, and a Cohen's d threshold of 1.41) revealed a significant phase shift between positions 1 and 2, and 1 and 3 for 8 Hz- and 10 Hz-induced frequencies (**Figure 3C,D**). We found no significant phase shift for 4 Hz- and 6 Hz-induced frequencies (**Figure 3A,B**). Together, the results demonstrate that the optimal phase of alpha perceptual cycles shifted across target positions, suggesting that the alpha-induced oscillations traveled across the retinotopic cortical space. This effect cannot merely be explained by low-level luminance masking as confirmed with a control experiment (see **Supplemental Information, Control experiment**) nor by a decreased phase estimation accuracy at low frequencies (see **Supplemental Information, Figure S1,** showing that the amplitude modulation is in fact higher at low compared to high induced frequency).

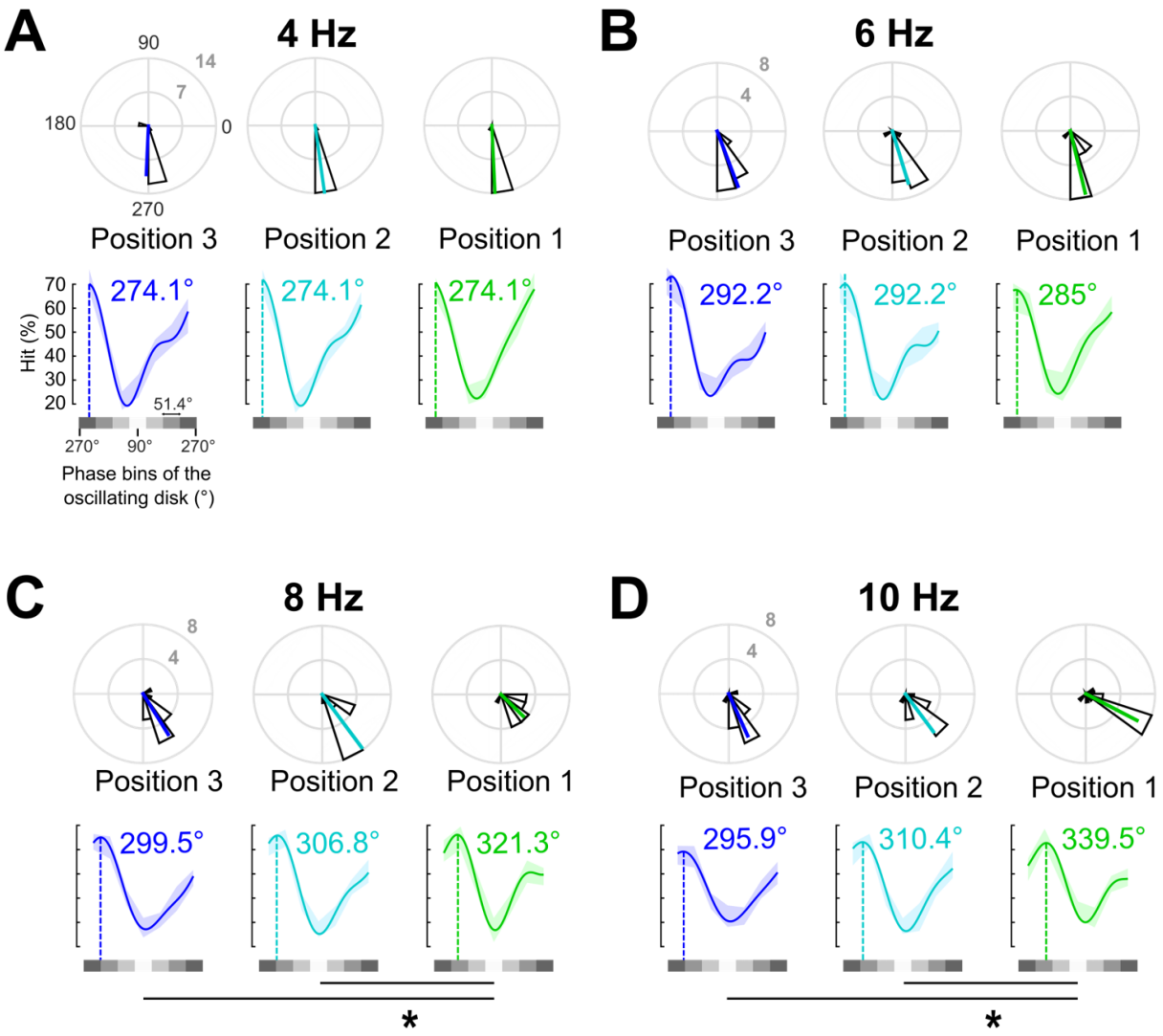

Figure 3. The optimal phase of alpha perceptual cycles shifts between target positions. *Lower graph of each panel, hit rate averaged across participants (n=15), binned as a function of the phase of the oscillating disk, and fitted to a complex sine function. Shaded colored area, 95 confidence intervals. Solid line, sine fit. Dotted line, optimal phase in degrees. Top graph of each panel, rose plot distribution of the optimal phase across participants. Colored solid line, optimal phase averaged across participants. Gray scale, phase bins of the oscillating disk. Each bin represents 51.4° of the oscillatory cycle.* ***A.*** *results for induced frequencies of* ***A.*** *4,* ***B.*** *6,* ***C.*** *8 and* ***D.*** *10 Hz. Performance was significantly modulated periodically at each target position and frequency (Monte Carlo, Bonferroni corrected across target positions and frequencies, p-value threshold < 0.01). The optimal phase shifted between positions 1 and 2, and 1 and 3 for 8 Hz- and 10 Hz-induced frequencies (Monte Carlo, FDR corrected, p-value threshold of 0.01). There was no significant phase shift for 4 Hz- and 6 Hz-induced frequencies.*

Finally, when converting the phase shift observed between target positions 1 and 2, and 1 and 3 into milliseconds (5 ms and 8 ms for 8 Hz, and 8 ms and 12 ms for 10 Hz, respectively) and

given the cortical distance between two target positions (0.8 mm distance edge-to-edge) as well as the targets' cortical size (0.8 mm diameter), one can estimate that alpha-induced brain oscillations traveled across the retinotopic space at a propagation speed ranging from 0.2 to 0.4 m/s.

Discussion

Using psychophysics and EEG, we investigated whether perceptual cycles travel across the retinotopic space in humans. The results showed that visual perception at each target position is modulated periodically at the induced frequency, replicating previous results [31-38]. Critically, the optimal phase for visual perception shifted between the target position closest to the inducer and the more distant targets. This effect was observed exclusively for alpha frequencies (8 Hz and 10 Hz; and cannot be simply explained by a mere luminance masking confound), with a propagation speed of 0.2-0.4 m/s. Together, the results support the hypothesis that alpha-induced brain oscillations travel across the visual cortex to modulate performance periodically across space and time.

Neural traveling waves, a growing, yet largely understudied field. A traveling wave is the propagation of neural activity over space with a constant shift in the peak latency between the origin of the signal and more distal positions [39, 40]. A growing literature reports that neural activity can travel *between* cortical areas, so-called macroscopic traveling waves. Monkey electrophysiology studies revealed that alpha oscillations travel between visual regions from V4 to V1, while gamma oscillations travel from V1 to V4 [41]. In humans, macroscopic oscillatory traveling waves have been reported using invasive (electrocorticography, ECoG, [42-47]) and non-invasive (EEG, e.g., [44, 48-60]; MEG, [44, 61-64]) recordings.

Critically, mesoscopic waves [39, 40] travel *within* individual brain regions (e.g., V1) spanning millimeters. Studies using invasive recordings with high spatial and temporal resolution (Local field potential, LFP; Multielectrode arrays, MEAs; Voltage-sensitive dyes, VSDs) showed non-oscillatory traveling activity in visual cortices of mammals (cats, monkeys, rats) (anesthetized:

[65-75]; awake: [76-82]). Mesoscopic non-oscillatory traveling waves have also been observed in non-visual, sensory, and motor cortices of mammals (cats, rats, guinea pigs, monkeys) (anesthetized: [83-89]; awake: [90-94]), and in reptiles (salamander) (anesthetized: [95-97]). Much fewer studies have focused on mesoscopic oscillatory traveling waves. They showed that delta (0.5-4 Hz), theta (4-7 Hz), alpha (8-14 Hz), beta (15-30 Hz) and gamma (>30 Hz) oscillations can propagate within individual visual areas of mammals and turtles [14-24, 98, 99]. Low-frequency oscillations were shown to also propagate in the olfactory bulb and cortex [100, 101]; and beta oscillations in the motor cortex [102, 103]. In humans, only a few studies, using invasive recordings in patients, showed the propagation of theta, alpha, and beta mesoscopic traveling waves [25-27], but only in non-visual cortical areas. There is no electro-physiological study to date investigating the propagation of low-frequency oscillations in individual human visual areas.

Finally, if a few studies have investigated the functional role of propagating oscillatory activity at the macroscopic (memory: [47, 51, 52]; attention: [41, 53]; saccadic eye movements: [60]; visual perception: [48, 49, 54-59]), and mesoscopic levels (attention: [19]; memory: [17]; motricity: [25, 102]; saccadic eye movements: [24]; visual perception: [23, 104]), very little is known about the link between oscillatory activity propagation within individual visual areas and perceptual performance, especially in human.

The present study builds on [28] and addresses this clear gap in the literature. Using psychophysics, we showed that alpha-induced oscillations travel within individual visual areas, leading perceptual cycles to travel across the retinotopic space.

Oscillatory Mesoscopic Traveling Waves in visual areas have clear perceptual consequences. Sokoliuk and VanRullen [28] (2016) reasoned that were an induced-oscillation propagated across the visual cortex, it should have perceptual consequences across the retinotopic visual space. Using a similar psychophysical paradigm, they found a shift of the behavioral optimal phase as a function of distance from the inducer. Contrary to our results, however, they observed this effect for both frequencies of 5 Hz (theta) and 10 Hz (alpha), but not 15 Hz, while

here we show a shift exclusively for alpha-induced frequencies (8 Hz and 10 Hz; but not 4 Hz and 6 Hz). These discrepant results can be explained by a number of critical differences between the two studies. First, our EEG results revealed that the oscillating disk produced a complex neural response composed of the induced frequency and its first harmonic, coherent with the nature of the visual system [29, 30, 36]. Thus, one must fit the behavioral response with a corresponding complex sine function to accurately capture the non-linearity of the neural response. Since the EEG was not recorded in Sokoliuk and VanRullen [28] (2016), the shape of the induced oscillation was unknown. Second, to ensure that the three targets activated the same number neurons in the visual regions, hence landing in a similar spatial extent (spatial phase) of the traveling wave, we adjusted the size of each target to cortical magnification. Third, in our study, the same participants (n=15) performed all four frequency conditions thus ensuring equal statistical power and no inter-participant variability (n=5 for 5 Hz, n=7 for 10 Hz and n=15 for a 10-Hz replication set, and n=4 for 15Hz in [28]). Finally, we used eye-tracking to ensure stable fixation, critical when investigating retinotopic propagation.

Propagation of alpha but not theta oscillations. Attention is the cognitive function that selects relevant information to facilitate its processing while still being able to flexibly redeploy resources to other information if necessary [105-107]. Studies have shown that when covert attention (in the absence of head or eye movements) is sustained at a given spatial location, information is sampled periodically at the alpha frequency (review [11, 108]). In other words, visual performance fluctuates over time along with the phase of alpha oscillations, in detection tasks in which the target stimulus appeared always at the same spatial location [1-3, 5-8, 13]. However, when multiple stimuli are presented, attention rhythmically samples information at the theta frequency [4, 9, 109-113] (review [10, 11, 108]).

Here, while we did not explicitly manipulate covert attention, participants fixated at the center of the screen and targets appeared in a constrained location suggesting that covert, voluntary spatial attention was sustained on the bottom right quadrant. This manipulation likely recruited alpha sampling, which potentially favored the propagation of alpha-induced oscillations

(although alpha-induced oscillations could also potentially travel in the absence of attention). One can speculate that the propagation of alpha oscillations away from the main attention focus could allow the observer to periodically monitor other nearby locations allowing for flexible attentional reallocation when a target appears. Further studies are necessary to investigate this hypothesis.

Speed and spatial extent of mesoscopic traveling waves. Our results show that alpha waves travel across the retinotopic space at a propagation speed of 0.2-0.4 m/s. Such observation is in line with results from the animal literature showing that transient neural signals travel within visual regions at a propagation speed of 0.06-0.4 m/s (0.2 m/s on average) from ~2 mm to ~7 mm of cortex [66-68, 70-79, 81, 82], as well as with studies showing that low-frequency oscillations propagate within visual areas at a speed of 0.01-0.6 m/s (0.25 m/s on average) [14, 16-18, 21, 23, 24, 98, 99]. Additionally, given a phase difference of ~7° to ~30° between target positions, it is unlikely that more than one (spatial) cycle (360°) of oscillatory activity propagates across such a small portion of the visual cortex (see **Figure 1**), in line with previous observations [24, 26].

Finally, given our specific manipulation (contrast change) and the observed propagation of perceptual cycles, it is likely that our paradigm has preferentially probed alpha traveling waves in area V1 (with small receptive fields). Studies, however, have shown that a single visual stimulation can propagate simultaneously within several brain areas, e.g., V1 and V2 [21], suggesting that this simultaneity may be crucial for the integration of retinotopic information in parallel, across multiple visual areas [21]. Future electrophysiological studies are necessary to validate this hypothesis.

Conclusion. Using a carefully designed psychophysical protocol, combined with EEG and eye-tracking, our study demonstrates that alpha perceptual cycles travel across the retinotopic visual space in humans, at a propagation speed of 0.2-0.4 m/s. These results suggest that alpha-induced brain oscillations travel across the visual cortex to modulate performance periodically across space and time.

References

1. Busch, N.A., Dubois, J., and VanRullen, R. (2009). The Phase of Ongoing EEG Oscillations Predicts Visual Perception. J. Neurosci. 29, 7869–7876.

2. Mathewson, K.E., Gratton, G., Fabiani, M., Beck, D.M., and Ro, T. (2009). To See or Not to See: Prestimulus α Phase Predicts Visual Awareness. J. Neurosci. 29, 2725–2732.

3. Valera, F.J., Toro, A., Roy John, E., and Schwartz, E.L. (1981). Perceptual framing and cortical alpha rhythm. Neuropsychologia 19, 675–686.

4. Dugué, L., Marque, P., and VanRullen, R. (2015). Theta Oscillations Modulate Attentional Search Performance Periodically. Journal of Cognitive Neuroscience 27, 945–958.

5. Dugué, L., Marque, P., and VanRullen, R. (2011). The Phase of Ongoing Oscillations Mediates the Causal Relation between Brain Excitation and Visual Perception. J. Neurosci. 31, 11889–11893.

6. Samaha, J., Gosseries, O., and Postle, B.R. (2017). Distinct Oscillatory Frequencies Underlie Excitability of Human Occipital and Parietal Cortex. J. Neurosci. 37, 2824–2833.

7. Samaha, J., and Postle, B.R. (2015). The Speed of Alpha-Band Oscillations Predicts the Temporal Resolution of Visual Perception. Current Biology 25, 2985–2990.

8. Fakche, C., VanRullen, R., Marque, P., and Dugué, L. (2022). α Phase-Amplitude Tradeoffs Predict Visual Perception. eNeuro. 1-16.

9. Merholz, G., Grabot, L., VanRullen, R., and Dugué, L. (2022). Periodic attention operates faster during more complex visual search. Scientific Reports. 12(1), 1-14.

10. VanRullen, R. (2016). Perceptual Cycles. Trends in Cognitive Sciences. 20, 723–735.

11. Kienitz, R., Schmid, M.C., and Dugué, L. Rhythmic sampling revisited: Experimental paradigms and neural mechanisms. European Journal of Neuroscience n/a.

12. Baumgarten, T.J., Schnitzler, A., and Lange, J. (2015). Beta oscillations define discrete perceptual cycles in the somatosensory domain. PNAS 112, 12187–12192.

13. Busch, N.A., and VanRullen, R. (2010). Spontaneous EEG oscillations reveal periodic sampling of visual attention. PNAS 107, 16048–16053.

14. Sanchez-Vives, M.V., and McCormick, D.A. (2000). Cellular and network mechanisms of rhythmic recurrent activity in neocortex. Nat Neurosci 3, 1027–1034.

15. Huang, X., Troy, W.C., Yang, Q., Ma, H., Laing, C.R., Schiff, S.J., and Wu, J.-Y. (2004). Spiral Waves in Disinhibited Mammalian Neocortex. J. Neurosci. 24, 9897–9902.

16. Benucci, A., Frazor, R.A., and Carandini, M. (2007). Standing Waves and Traveling Waves Distinguish Two Circuits in Visual Cortex. Neuron 55, 103–117.

17. Han, F., Caporale, N., and Dan, Y. (2008). Reverberation of Recent Visual Experience in Spontaneous Cortical Waves. Neuron 60, 321–327.

18. Ray, S., and Maunsell, J.H.R. (2011). Different Origins of Gamma Rhythm and High-Gamma Activity in Macaque Visual Cortex. PLOS Biology 9, e1000610, 1-9.

19. Maris, E., Womelsdorf, T., Desimone, R., and Fries, P. (2013). Rhythmic neuronal synchronization in visual cortex entails spatial phase relation diversity that is modulated by stimulation and attention. NeuroImage 74, 99–116.

20. Stroh, A., Adelsberger, H., Groh, A., Rühlmann, C., Fischer, S., Schierloh, A., Deisseroth, K., and Konnerth, A. (2013). Making Waves: Initiation and Propagation of Corticothalamic Ca2+ Waves In Vivo. Neuron 77, 1136–1150.

21. Muller, L., Reynaud, A., Chavane, F., and Destexhe, A. (2014). The stimulus-evoked population response in visual cortex of awake monkey is a propagating wave. Nat Commun 5(1), 1-14.

22. Townsend, R.G., Solomon, S.S., Chen, S.C., Pietersen, A.N.J., Martin, P.R., Solomon, S.G., and Gong, P. (2015). Emergence of Complex Wave Patterns in Primate Cerebral Cortex. J. Neurosci. 35, 4657–4662.

23. Davis, Z.W., Muller, L., Martinez-Trujillo, J., Sejnowski, T., and Reynolds, J.H. (2020). Spontaneous travelling cortical waves gate perception in behaving primates. Nature 587, 432–436.

24. Zanos, T.P., Mineault, P.J., Nasiotis, K.T., Guitton, D., and Pack, C.C. (2015). A Sensorimotor Role for Traveling Waves in Primate Visual Cortex. Neuron 85, 615–627.

25. Takahashi, K., Saleh, M., Penn, R., and Hatsopoulos, N. (2011). Propagating Waves in Human Motor Cortex. Frontiers in Human Neuroscience 5, 1-8.

26. Zhang, H., and Jacobs, J. (2015). Traveling Theta Waves in the Human Hippocampus. J. Neurosci. 35, 12477–12487.

27. Sreekumar, V., Wittig, J.H., Chapeton, J.I., Inati, S.K., and Zaghloul, K.A. (2021). Low frequency traveling waves in the human cortex coordinate neural activity across spatial scales. BioRxiv, 1-48.

28. Sokoliuk, R., and VanRullen, R. (2016). Global and local oscillatory entrainment of visual behavior across retinotopic space. Sci Rep 6(1), 1-12

29. Heinrich, S.P. (2010). Some thoughts on the interpretation of steady-state evoked potentials. Doc Ophthalmol 120, 205–214.

30. Norcia, A.M., Appelbaum, L.G., Ales, J.M., Cottereau, B.R., and Rossion, B. (2015). The steady-state visual evoked potential in vision research: A review. Journal of Vision 15(6), 4-4

31. Stefanics, G., Hangya, B., Hernádi, I., Winkler, I., Lakatos, P., and Ulbert, I. (2010). Phase Entrainment of Human Delta Oscillations Can Mediate the Effects of Expectation on Reaction Speed. J. Neurosci. 30, 13578–13585.

32. Mathewson, K.E., Prudhomme, C., Fabiani, M., Beck, D.M., Lleras, A., and Gratton, G. (2012). Making Waves in the Stream of Consciousness: Entraining Oscillations in EEG Alpha and Fluctuations in Visual Awareness with Rhythmic Visual Stimulation. Journal of Cognitive Neuroscience 24, 2321–2333.

33. Henry, M.J., and Obleser, J. (2012). Frequency modulation entrains slow neural oscillations and optimizes human listening behavior. PNAS 109, 20095–20100.

34. Henry, M.J., Herrmann, B., and Obleser, J. (2014). Entrained neural oscillations in multiple frequency bands comodulate behavior. PNAS 111, 14935–14940.

35. Graaf, T.A. de, Gross, J., Paterson, G., Rusch, T., Sack, A.T., and Thut, G. (2013). Alpha-Band Rhythms in Visual Task Performance: Phase-Locking by Rhythmic Sensory Stimulation. PLOS ONE 8, e60035, 1-12.

36. Spaak, E., Lange, F.P. de, and Jensen, O. (2014). Local Entrainment of Alpha Oscillations by Visual Stimuli Causes Cyclic Modulation of Perception. J. Neurosci. 34, 3536–3544.

37. Oever, S. ten, and Sack, A.T. (2015). Oscillatory phase shapes syllable perception. PNAS 112, 15833–15837.

38. Kizuk, S.A.D., and Mathewson, K.E. (2017). Power and Phase of Alpha Oscillations Reveal an Interaction between Spatial and Temporal Visual Attention. Journal of Cognitive Neuroscience 29, 480–494.

39. Sato, T.K., Nauhaus, I., and Carandini, M. (2012). Traveling Waves in Visual Cortex. Neuron 75, 218–229.

40. Muller, L., Chavane, F., Reynolds, J., and Sejnowski, T.J. (2018). Cortical travelling waves: mechanisms and computational principles. Nat Rev Neurosci 19, 255–268.

41. Kerkoerle, T. van, Self, M.W., Dagnino, B., Gariel-Mathis, M.-A., Poort, J., Togt, C. van der, and Roelfsema, P.R. (2014). Alpha and gamma oscillations characterize feedback and feedforward processing in monkey visual cortex. PNAS 111, 14332–14341.

42. Nir, Y., Staba, R.J., Andrillon, T., Vyazovskiy, V.V., Cirelli, C., Fried, I., and Tononi, G. (2011). Regional Slow Waves and Spindles in Human Sleep. Neuron 70, 153–169.

43. Meij, R. van der, Kahana, M., and Maris, E. (2012). Phase–Amplitude Coupling in Human Electrocorticography Is Spatially Distributed and Phase Diverse. J. Neurosci. 32, 111–123.

44. Alexander, D.M., Jurica, P., Trengove, C., Nikolaev, A.R., Gepshtein, S., Zvyagintsev, M., Mathiak, K., Schulze-Bonhage, A., Ruescher, J., Ball, T., et al. (2013). Traveling waves and trial averaging: The nature of single-trial and averaged brain responses in large-scale cortical signals. NeuroImage 73, 95–112.

45. Bahramisharif, A., Gerven, M.A.J. van, Aarnoutse, E.J., Mercier, M.R., Schwartz, T.H., Foxe, J.J., Ramsey, N.F., and Jensen, O. (2013). Propagating Neocortical Gamma Bursts Are Coordinated by Traveling Alpha Waves. J. Neurosci. 33, 18849–18854.

46. Muller, L., Piantoni, G., Koller, D., Cash, S.S., Halgren, E., and Sejnowski, T.J. (2016). Rotating waves during human sleep spindles organize global patterns of activity that repeat precisely through the night. eLife 5, e17267, 1-16.

47. Zhang, H., Watrous, A.J., Patel, A., and Jacobs, J. (2018). Theta and Alpha Oscillations Are Traveling Waves in the Human Neocortex. Neuron 98, 1269-1281.e4.

48. Schack, B., Weiss, S., and Rappelsberger, P. (2003). Cerebral information transfer during word processing: Where and when does it occur and how fast is it? Human Brain Mapping 19, 18–36.

49. Shevelev, I.A., Kamenkovich, V.M., Bark, E.D., Verkhlutov, V.M., Sharaev, G.A., and Mikhailova, E.S. (2000). Visual illusions and travelling alpha waves produced by flicker at alpha frequency. International Journal of Psychophysiology 39, 9–20.

50. Burkitt, G.R., Silberstein, R.B., Cadusch, P.J., and Wood, A.W. (2000). Steady-state visual evoked potentials and travelling waves. Clinical Neurophysiology 111, 246–258.

51. Sauseng, P., Klimesch, W., Gruber, W., Doppelmayr, M., Stadler, W., and Schabus, M. (2002). The interplay between theta and alpha oscillations in the human electroencephalogram reflects the transfer of information between memory systems. Neuroscience Letters 324, 121–124.

52. Alexander, D.M., Arns, M.W., Paul, R.H., Rowe, D.L., Cooper, N., Esser, A.H., Fallahpour, K., Stephan, B.C.M., Heesen, E., Breteler, R., et al. (2006). Eeg markers for cognitive decline in elderly subjects with subjective memory complaints. J. Integr. Neurosci. 05, 49–74.

53. Alexander, D.M., Hermens, D.F., Keage, H.A.D., Clark, C.R., Williams, L.M., Kohn, M.R., Clarke, S.D., Lamb, C., and Gordon, E. (2008). Event-related wave activity in the EEG provides new marker of ADHD. Clinical Neurophysiology 119, 163–179.

54. Patten, T.M., Rennie, C.J., Robinson, P.A., and Gong, P. (2012). Human Cortical Traveling Waves: Dynamical Properties and Correlations with Responses. PLOS ONE 7, e38392, 1-10.

55. Fellinger, R., Gruber, W., Zauner, A., Freunberger, R., and Klimesch, W. (2012). Evoked traveling alpha waves predict visual-semantic categorization-speed. NeuroImage 59, 3379–3388.

56. Alamia, A., and VanRullen, R. (2019). Alpha oscillations and traveling waves: Signatures of predictive coding? PLOS Biology 17, e3000487, 1-26.

57. Lozano-Soldevilla, D., and VanRullen, R. (2019). The Hidden Spatial Dimension of Alpha: 10-Hz Perceptual Echoes Propagate as Periodic Traveling Waves in the Human Brain. Cell Reports 26, 374-380.e4.

58. Pang (庞兆阳), Z., Alamia, A., and VanRullen, R. (2020). Turning the Stimulus On and Off Changes the Direction of α Traveling Waves. eNeuro 7, 1-11.

59. King, J.-R., and Wyart, V. (2021). The Human Brain Encodes a Chronicle of Visual Events at Each Instant of Time Through the Multiplexing of Traveling Waves. J. Neurosci. 41, 7224–7233.

60. Giannini, M., Alexander, D.M., Nikolaev, A.R., and van Leeuwen, C. (2018). Large-Scale Traveling Waves in EEG Activity Following Eye Movement. Brain Topogr 31, 608–622.

61. Ribary, U., Ioannides, A.A., Singh, K.D., Hasson, R., Bolton, J.P., Lado, F., Mogilner, A., and Llinás, R. (1991). Magnetic field tomography of coherent thalamocortical 40-Hz oscillations in humans. PNAS 88, 11037–11041.

62. Thorpe, S.G., Nunez, P.L., and Srinivasan, R. (2007). Identification of wave-like spatial structure in the SSVEP: Comparison of simultaneous EEG and MEG. Statistics in Medicine 26, 3911–3926.

63. Cottereau, B., Lorenceau, J., Gramfort, A., Clerc, M., Thirion, B., and Baillet, S. (2011). Phase delays within visual cortex shape the response to steady-state visual stimulation. NeuroImage 54, 1919–1929.

64. van Ede, F., van Pelt, S., Fries, P., and Maris, E. (2015). Both ongoing alpha and visually induced gamma oscillations show reliable diversity in their across-site phase-relations. Journal of Neurophysiology 113, 1556–1563.

65. Bringuier, V., Chavane, F., Glaeser, L., and Frégnac, Y. (1999). Horizontal Propagation of Visual Activity in the Synaptic Integration Field of Area 17 Neurons. Science 283, 695–699.

66. Jancke, D., Chavane, F., Naaman, S., and Grinvald, A. (2004). Imaging cortical correlates of illusion in early visual cortex. Nature 428, 423–426.

67. Roland, P.E., Hanazawa, A., Undeman, C., Eriksson, D., Tompa, T., Nakamura, H., Valentiniene, S., and Ahmed, B. (2006). Cortical feedback depolarization waves: A mechanism of top-down influence on early visual areas. PNAS 103, 12586–12591.

68. Lippert, M.T., Takagaki, K., Xu, W., Huang, X., and Wu, J.-Y. (2007). Methods for Voltage-Sensitive Dye Imaging of Rat Cortical Activity With High Signal-to-Noise Ratio. Journal of Neurophysiology 98, 502–512.

69. Sharon, D., Jancke, D., Chavane, F., Na'aman, S., and Grinvald, A. (2007). Cortical Response Field Dynamics in Cat Visual Cortex. Cerebral Cortex 17, 2866–2877.

70. Xu, W., Huang, X., Takagaki, K., and Wu, J. (2007). Compression and Reflection of Visually Evoked Cortical Waves. Neuron 55, 119–129.

71. Takagaki, K., Zhang, C., Wu, J.-Y., and Lippert, M.T. (2008). Crossmodal propagation of sensory-evoked and spontaneous activity in the rat neocortex. Neuroscience Letters 431, 191–196.

72. Nauhaus, I., Busse, L., Ringach, D.L., and Carandini, M. (2012). Robustness of Traveling Waves in Ongoing Activity of Visual Cortex. J. Neurosci. 32, 3088–3094.

73. Nauhaus, I., Busse, L., Carandini, M., and Ringach, D.L. (2009). Stimulus contrast modulates functional connectivity in visual cortex. Nat Neurosci 12, 70–76.

74. Gao, X., Xu, W., Wang, Z., Takagaki, K., Li, B., and Wu, J. -y. (2012). Interactions between two propagating waves in rat visual cortex. Neuroscience 216, 57–69.

75. Rekauzke, S., Nortmann, N., Staadt, R., Hock, H.S., Schöner, G., and Jancke, D. (2016). Temporal Asymmetry in Dark–Bright Processing Initiates Propagating Activity across Primary Visual Cortex. J. Neurosci. 36, 1902–1913.

76. Slovin, H., Arieli, A., Hildesheim, R., and Grinvald, A. (2002). Long-Term Voltage-Sensitive Dye Imaging Reveals Cortical Dynamics in Behaving Monkeys. Journal of Neurophysiology 88, 3421–3438.

77. Chen, Y., Geisler, W.S., and Seidemann, E. (2006). Optimal decoding of correlated neural population responses in the primate visual cortex. Nat Neurosci 9, 1412–1420.

78. Sit, Y.F., Chen, Y., Geisler, W.S., Miikkulainen, R., and Seidemann, E. (2009). Complex Dynamics of V1 Population Responses Explained by a Simple Gain-Control Model. Neuron 64, 943–956.

79. Reynaud, A., Masson, G.S., and Chavane, F. (2012). Dynamics of Local Input Normalization Result from Balanced Short- and Long-Range Intracortical Interactions in Area V1. J. Neurosci. 32, 12558–12569.

80. Zhang, Q., Wen, Y., Zhang, D., She, L., Wu, J., Dan, Y., and Poo, M. (2012). Priming with real motion biases visual cortical response to bistable apparent motion. PNAS 109, 20691–20696.

81. Yang, Z., Heeger, D.J., Blake, R., and Seidemann, E. (2015). Long-range traveling waves of activity triggered by local dichoptic stimulation in V1 of behaving monkeys. Journal of Neurophysiology 113, 277–294.

82. Chemla, S., Reynaud, A., Volo, M. di, Zerlaut, Y., Perrinet, L., Destexhe, A., and Chavane, F. (2019). Suppressive Traveling Waves Shape Representations of Illusory Motion in Primary Visual Cortex of Awake Primate. J. Neurosci. 39, 4282–4298.

83. Petersen, C.C.H., Grinvald, A., and Sakmann, B. (2003). Spatiotemporal Dynamics of Sensory Responses in Layer 2/3 of Rat Barrel Cortex Measured In Vivo by Voltage-Sensitive Dye Imaging Combined with Whole-Cell Voltage Recordings and Neuron Reconstructions. J. Neurosci. 23, 1298–1309.

84. Derdikman, D., Hildesheim, R., Ahissar, E., Arieli, A., and Grinvald, A. (2003). Imaging Spatiotemporal Dynamics of Surround Inhibition in the Barrels Somatosensory Cortex. J. Neurosci. 23, 3100–3105.

85. Tsytsarev, V., Yamazaki, T., Ribot, J., and Tanaka, S. (2004). Sound frequency representation in cat auditory cortex. NeuroImage 23, 1246–1255.

86. Civillico, E.F., and Contreras, D. (2006). Integration of Evoked Responses in Supragranular Cortex Studied With Optical Recordings In Vivo. Journal of Neurophysiology 96, 336–351.

87. Song, W.-J., Kawaguchi, H., Totoki, S., Inoue, Y., Katura, T., Maeda, S., Inagaki, S., Shirasawa, H., and Nishimura, M. (2006). Cortical Intrinsic Circuits Can Support Activity Propagation through an Isofrequency Strip of the Guinea Pig Primary Auditory Cortex. Cerebral Cortex 16, 718–729.

88. Nishimura, M., Shirasawa, H., Kaizo, H., and Song, W.-J. (2007). New Field With Tonotopic Organization in Guinea Pig Auditory Cortex. Journal of Neurophysiology 97, 927–932.

89. Reimer, A., Hubka, P., Engel, A.K., and Kral, A. (2011). Fast Propagating Waves within the Rodent Auditory Cortex. Cerebral Cortex 21, 166–177.

90. Petersen, C.C.H., Hahn, T.T.G., Mehta, M., Grinvald, A., and Sakmann, B. (2003). Interaction of sensory responses with spontaneous depolarization in layer 2/3 barrel cortex. PNAS 100, 13638–13643.

91. Ferezou, I., Haiss, F., Gentet, L.J., Aronoff, R., Weber, B., and Petersen, C.C.H. (2007). Spatiotemporal Dynamics of Cortical Sensorimotor Integration in Behaving Mice. Neuron 56, 907–923.

92. Ferezou, I., Bolea, S., and Petersen, C.C.H. (2006). Visualizing the Cortical Representation of Whisker Touch: Voltage-Sensitive Dye Imaging in Freely Moving Mice. Neuron 50, 617–629.

93. Luczak, A., Barthó, P., Marguet, S.L., Buzsáki, G., and Harris, K.D. (2007). Sequential structure of neocortical spontaneous activity in vivo. PNAS 104, 347–352.

94. Witte, R.S., Rousche, P.J., and Kipke, D.R. (2007). Fast wave propagation in auditory cortex of an awake cat using a chronic microelectrode array. J. Neural Eng. 4, 68–78.

95. Cinelli, A.R., Hamilton, K.A., and Kauer, J.S. (1995). Salamander olfactory bulb neuronal activity observed by video rate, voltage-sensitive dye imaging. III. Spatial and temporal properties of responses evoked by odorant stimulation. Journal of Neurophysiology 73, 2053–2071.

96. Cinelli, A.R., and Kauer, J.S. (1995). Salamander olfactory bulb neuronal activity observed by video rate, voltage-sensitive dye imaging. II. Spatial and temporal properties of responses evoked by electric stimulation. Journal of Neurophysiology 73, 2033–2052.

97. Orbach, H.S., and Cohen, L.B. (1983). Optical monitoring of activity from many areas of the in vitro and in vivo salamander olfactory bulb: a new method for studying functional organization in the vertebrate central nervous system. J. Neurosci. 3, 2251–2262.

98. Prechtl, J.C., Bullock, T.H., and Kleinfeld, D. (2000). Direct evidence for local oscillatory current sources and intracortical phase gradients in turtle visual cortex. PNAS 97, 877–882.

99. Prechtl, J.C., Cohen, L.B., Pesaran, B., Mitra, P.P., and Kleinfeld, D. (1997). Visual stimuli induce waves of electrical activity in turtle cortex. PNAS 94, 7621–7626.

100. Lam, Y.-W., Cohen, L.B., and Zochowski, M.R. (2003). Odorant specificity of three oscillations and the DC signal in the turtle olfactory bulb. European Journal of Neuroscience 17, 436–446.

101. Lam, Y.-W., Cohen, L.B., Wachowiak, M., and Zochowski, M.R. (2000). Odors Elicit Three Different Oscillations in the Turtle Olfactory Bulb. J. Neurosci. 20, 749–762.

102. Rubino, D., Robbins, K.A., and Hatsopoulos, N.G. (2006). Propagating waves mediate information transfer in the motor cortex. Nat Neurosci 9, 1549–1557.

103. Takahashi, K., Kim, S., Coleman, T.P., Brown, K.A., Suminski, A.J., Best, M.D., and Hatsopoulos, N.G. (2015). Large-scale spatiotemporal spike patterning consistent with wave propagation in motor cortex. Nat Commun 6, 7169, 1-11.

104. Besserve, M., Lowe, S.C., Logothetis, N.K., Schölkopf, B., and Panzeri, S. (2015). Shifts of Gamma Phase across Primary Visual Cortical Sites Reflect Dynamic Stimulus-Modulated Information Transfer. PLOS Biology 13, e1002257, 1-29.

105. Carrasco, M. (2011). Visual attention: The past 25 years. Vision Research 51, 1484–1525.

106. Dugué, L., Merriam, E.P., Heeger, D.J., and Carrasco, M. (2020). Differential impact of endogenous and exogenous attention on activity in human visual cortex. Sci Rep 10, 21274, 1-16.

107. Dugué, L., Merriam, E.P., Heeger, D.J., and Carrasco, M. (2018). Specific Visual Subregions of TPJ Mediate Reorienting of Spatial Attention. Cerebral Cortex 28, 2375–2390.

108. Dugué, L., and VanRullen, R. (2017). Transcranial Magnetic Stimulation Reveals Intrinsic Perceptual and Attentional Rhythms. Frontiers in Neuroscience 11, 1-7.

109. Landau, A.N., and Fries, P. (2012). Attention Samples Stimuli Rhythmically. Current Biology 22, 1000–1004.

110. Fiebelkorn, I.C., Saalmann, Y.B., and Kastner, S. (2013). Rhythmic Sampling within and between Objects despite Sustained Attention at a Cued Location. Current Biology 23, 2553–2558.

111. Song, K., Meng, M., Chen, L., Zhou, K., and Luo, H. (2014). Behavioral Oscillations in Attention: Rhythmic α Pulses Mediated through θ Band. J. Neurosci. 34, 4837–4844.

112. Huang, Y., Chen, L., and Luo, H. (2015). Behavioral Oscillation in Priming: Competing Perceptual Predictions Conveyed in Alternating Theta-Band Rhythms. J. Neurosci. 35, 2830–2837.

113. Dugué, L., Beck, A.-A., Marque, P., and VanRullen, R. (2019). Contribution of FEF to Attentional Periodicity during Visual Search: A TMS Study. eNeuro 6, 1-10.

114. Strasburger, H., Rentschler, I., and Jüttner, M. (2011). Peripheral vision and pattern recognition: A review. Journal of vision, 11(5):13, 1-82.

115. Delorme, A., and Makeig, S. (2004). EEGLAB: an open source toolbox for analysis of single-trial EEG dynamics including independent component analysis. Journal of Neuroscience Methods 134, 9–21.

116. Rossion, B., Prieto, E.A., Boremanse, A., Kuefner, D., and Van Belle, G. (2012). A steady-state visual evoked potential approach to individual face perception: Effect of inversion, contrast-reversal and temporal dynamics. NeuroImage 63, 1585–1600.

117. Liu-Shuang, J., Norcia, A.M., and Rossion, B. (2014). An objective index of individual face discrimination in the right occipito-temporal cortex by means of fast periodic oddball stimulation. Neuropsychologia 52, 57–72.

118. Vanrullen, R., and Dubois, J. (2011). The Psychophysics of Brain Rhythms. Front. Psychol. 1-10.

119. Carrasco, M., and McElree, B. (2001). Covert attention accelerates the rate of visual information processing. Proceedings of the National Academy of Sciences 98, 5363–5367.

120. Reed, A.V. (1973). Speed-accuracy trade-off in recognition memory. Science 181, 574–576.

121. Wickelgren, W.A. (1977). Speed-accuracy tradeoff and information processing dynamics. Acta Psychologica 41, 67–85.

122. Watt, J., Borhani, R., and Katsaggelos, A.K. (2020). Machine Learning Refined: Foundations, Algorithms, and Applications (Cambridge University Press).

123. Fawcett, I.P., Barnes, G.R., Hillebrand, A., and Singh, K.D. (2004). The temporal frequency tuning of human visual cortex investigated using synthetic aperture magnetometry. NeuroImage 21, 1542–1553.

124. Srinivasan, R., Fornari, E., Knyazeva, M.G., Meuli, R., and Maeder, P. (2007). fMRI responses in medial frontal cortex that depend on the temporal frequency of visual input. Exp Brain Res 180, 677–691.

125. Meteyard, L., and Davies, R.A.I. (2020). Best practice guidance for linear mixed-effects models in psychological science. Journal of Memory and Language 112, 104092, 1-83.

126. VanRullen, R. (2016). How to Evaluate Phase Differences between Trial Groups in Ongoing Electrophysiological Signals. Frontiers in Neuroscience 10.1-22.

127. Cohen, M.X. (2014). Analyzing Neural Time Series Data: Theory and Practice (MIT Press).

128. Berens, P. (2009). CircStat: A MATLAB Toolbox for Circular Statistics. Journal of Statistical Software 31, 1–21.

STAR Methods

Participants

18 participants (9 females, 16 right-handed, mean ± sd age: 26.2 ± 4.1 years) were recruited for the experiment. Three were excluded because they did not fulfill at least one of the analysis criteria (see analysis section below). 15 participants (7 females, 13 right-handed, mean ± sd age: 25.5 ± 3 years) were recruited for an additional control experiment (see **Supplemental Information**). All participants were free from medication affecting the central nervous system, reported no history of psychiatric or neurological disorders, gave their written informed consent and were compensated for their participation. The study was approved by the local French ethics committee Ouest IV (IRB #2020-A00859-30) and followed the Declaration of Helsinki.

Stimuli

Stimuli were designed with PsychToolbox 3.0.12, running in Matlab R2014b 64-bit (The MathWorks, Natick, MA), and displayed with a ProPixx Projector (VPixx Technologies, Saint-Bruno, QC, Canada), on a 139 x 77.5 cm projection screen (1920 x 1080 pixels; 480 Hz refresh rate), at 122 cm distance. Three different stimuli were generated: a fixation cross, a peripheral disk, and three small dots (targets). The arms of the fixation cross measured 0.15 degrees of visual angle (°) of length and 0.03° of width. The size and position of the targets were computed according to cortical magnification (Human cortical magnification factor = $\frac{23.07}{eccentricity + 0.75}$ [114]) so that each target (diameter) represented a 0.8 mm portion of cortex spaced by 0.8 mm edge-to-edge (radius: 0.09°, 0.1° and 0.12°; eccentricity: 4.1°, 4.5° and 4.9°). The peripheral disk (inducer) was displayed on the lower right corner at 7.5° of eccentricity (from the center of the disk; radius: 1.75°). The background color was black, and the fixation cross at 50% of contrast relative to the background. Target contrasts were titrated for each participant, each position, and each frequency, using a staircase procedure (see below). The peripheral disk was oscillating sinusoidally in luminance, from black to white (i.e., from 0% to 100% of contrast; one period: black-to-white-to-black), at frequencies in the theta and alpha range: 4.07, 6.13, 8.27 and 10.43 Hz. For clarity, we rounded these values to 4, 6, 8, and 10 Hz.

Eye tracker

Participant's head was maintained with a headrest and chinrest. An infrared video-camera system (EyeLink 1000 plus 5.08, SR Research, Ottawa, Canada) was used to ensure that participants maintained their gaze on the fixation cross throughout the block. The block only started when participants was successfully maintaining fixation. When a gaze deviation of >2° from the center of the screen was detected during the presentation of a target (-150 ms to +100 ms around target onset) or a blink, we considered that the participant broke fixation and the trial was removed from the analysis (112.6 ± 112.5 trials on average across participants, leading to a total number of trials of 5015.5 ± 209.8 trials per participant). Supernumerary

blocks were added at the end of each run to compensate for rejected trials. Participants received feedback at the end of each block to remind them to minimize blinking and to maintain fixation.

EEG

EEG was recorded using a 64-channels actiChamp system (Brain Products GmbH). The ground was placed at the Fpz position, and the right mastoid was used as reference (DC recording; 1000 Hz sampling rate).

Procedure

Participants performed five sessions: four psychophysics sessions (one sessions for each induced frequency; frequency order randomized across participants), and one EEG session. The psychophysics sessions were composed of the staircases and two runs of 50 blocks each. The EEG session contained four runs of 24 blocks each (one run for each induced frequency).

For both the staircases and the main task, each block lasted 30 seconds during which the peripheral disk continuously oscillated in luminance. 6 to 18 targets were presented at random times (excluding the first and the last seconds, and with at least one second interval between targets) during three frames (6.3 ms) according to a decreasing probability distribution (~10 targets per block on average). The number of targets for the three positions was randomized across blocks (and pseudorandomized across runs). Participants were instructed to press the space bar when they detected a target (in a 1-second time window after which their response was not considered; target presentation and response window composed a trial).

A one-up/one-down staircase with decreasing steps was performed separately for each target position to titrate the contrast of the target to reach about 50% detection. Each staircase was composed of 7 blocks, as described above, except that the targets appeared always at the same position. During the main task, target contrasts were adjusted every 15 blocks to maintain the same detection level across the entire session. Target contrasts averaged across participants were 2.59 ± 0.18 %, 1.83 ± 0.11 %, 2.37 ± 0.15 %, for position 1, 2, and 3,

respectively, for the 4 Hz-induced frequency; 2.77 ± 0.2 %, 1.9 ± 0.13 %, 2.41 ± 0.15 %, for position 1, 2, and 3, respectively, for 6 Hz; 2.09 ± 0.24 %, 1.94 ± 0.15 %, 2.43 ± 0.16 %, for position 1, 2, and 3, respectively, for 8 Hz; and 2.82 ± 0.3 %, 1.88 ± 0.16 %, 2.32 ± 0.14 %, for position 1, 2, and 3, respectively, for 10 Hz.

EEG Analysis

Analyses were performed with EEGLab 13.6.5 ([115]; Swartz Center for Computational Neuroscience, UC San Diego, California) running in Matlab.

Preprocessing. EEG data and channel location were imported into EEGLab. EEG data were re-referenced to the average of the right and left mastoids. A high-pass filter at 0.1 Hz and a notch filter between 48 and 52 Hz were applied, to respectively remove slow drifts and 50 Hz electric noise. The signal was further down sampled to 512 Hz. Visual inspection allowed to identify electrodes with low signal-to-noise ratio, which were then interpolated (spherical interpolation). Independent component analysis (ICA) was performed to remove blink components, after a visual inspection of their time courses and topographies. Data were epoched from trial onset (0s) to the end of the block (+30s).

Fast Fourier Transform. FFT were computed (Matlab function: fft) on epoched EEG data, and the amplitude was extracted for each electrode, epoch, and frequency. The signal-to-noise ratio (SNR) was computed on the amplitude extracted from the FFT, for each electrode, as the ratio of the amplitude at each frequency to the average of the 20 surroundings frequencies (10 frequencies on either side, excluding the immediately adjacent frequencies; note that the SNR could mathematically not be estimated at the edges of the spectra), as described in [116, 117]. SNR averaged across participants, epochs and electrodes were plotted to ensure that the oscillating disk successfully induced brain signal at the corresponding frequency. Topographies were plotted at the peak of the induced frequency and its first harmonic.

Event-Related Potentials (ERPs). Previously preprocessed EEG timeseries were further bandpass filtered between 1.5 Hz and 30 Hz, and baseline corrected from -400 to 0 ms from

block onset. Epochs of one second were defined, excluding the first second of each 30 seconds-block to avoid the transient EEG response due to stimulus onset. Participants' ERPs were computed as the averaged of all resulting epochs. ERPs averaged across participants for electrode Oz were plotted with the standard error of the mean. Electrode Oz was selected because it is the electrode with the highest amplitude across the four induced frequencies. The ERP plots allowed us to identify that the brain oscillation induced by the oscillating disk was a complex oscillation composed of the induced frequency and its first harmonic. Therefore, we fitted the behavioral data to a complex sine function.

FFT on ERPs. FFT was computed (1500 points zero padding) on the Oz ERP for each participant. The amplitude was extracted, and the SNR was computed as previously described.

Behavioral analysis

Behavioral analyses were performed with Matlab R2014b (The MathWorks, Natick, MA). The following dependent variables were computed: hit rates as main dependent variable, i.e., percentage of correct responses, and median reaction times as secondary dependent variables, for each target position and frequency. Hit rates averaged across frequencies were 47.55 ± 0.74 %, 45.75 ± 0.73 %, and 44.78 ± 0.69 % for position 1, 2, and 3, respectively. Median reaction times averaged across frequencies were 511 ± 8 ms, 512 ± 8 ms, and 510 ± 9 ms for position 1, 2, and 3, respectively. A two-way repeated-measures ANOVA was performed for each dependent variable to assess the effect of frequency and target position. For hit rates, there was a main effect of target position ($F(2, 28) = 11.02$, SS = 237.43, p-value < 0.01, $eta^2 = 44.04$) but no effect of frequency ($F(3, 42) = 0.45$, SS = 10.19, p-value = 0.71, $eta^2 = 3.15$) nor of their interaction ($F(6, 84) = 0.29$, SS = 10.82, p-value = 0.93). For median reaction times, there was a main effect of frequency ($F(3, 42) = 4.21$, SS = 5111.99, p-value = 0.01, $eta^2 = 23.14$), but no main effect of target position ($F(2, 28) = 0.34$, SS = 98.34, p-value = 0.71, $eta^2 = 2.39$), nor of their interaction ($F(6, 84) = 0.74$, SS = 456.48, p-value = 0.61). The absence of significant interaction between frequency and target positions in any of these two tests confirm successful contrast manipulation, i.e., the detection performance does not rely

on an interaction between frequency and target positions. As argued in [11] and [118], reaction time fluctuations do not unambiguously demonstrate rhythms in cognitive processes as they can also be the by-product of the external stimulation and are sensitive to changes in decision criteria [106, 107, 119-121]. The behavioral phase analyses thus focused on hit rates as the main dependent variable.

Phase effect on detection performance. Each target was assigned to one of 7 phase bins of the periodic stimulation depending on the delay at which they appeared during the block. Hit and false alarm rates were computed for each target position, frequency, and phase bin. For each block and target position, false alarms (participants reported perceiving a target while no target had been presented; participants were instructed to respond in the 1s-window following the target, after which the response was considered a false alarm) were binned as a function of the phase of the oscillating disk. To allow for a fair comparison between hit and false alarms, only the false alarms that were in the same phase bins as the targets (but in a different 100-ms period) were considered for further analysis (e.g., if 2 targets were presented at position 1 within the given block, and binned in bins number 2 and 6, only false alarms that were binned in bins number 2 and 6 were considered for further analysis). To allocate a false alarm to one of the three target positions (a false alarm is, by definition, at none of the position), a bootstrap procedure was performed (100 repetitions). One participant was excluded from the analysis at this point because the number of false alarms exceeded the number of targets presented.

Given the ERP results (see **Figure 2**) showing a complex neural response composed of the induced frequency and its first harmonic, behavioral data were fitted to a complex sine function (Eq1) with the following free parameters: $x[1]$ and $x[2]$ the amplitude and the phase offset of the induced frequency, respectively, $x[3]$ and $x[4]$ the amplitude and the phase offset of the first harmonic, respectively, and $x[5]$ the baseline level. To find the parameters that best fit the data, we used a Least Squares cost function, i.e., the cost function computed the total squared errors, i.e., the sum of squared errors, between the fit and the data, thus giving a measure of

how well the data are fitted. The best fit is the one whose parameters minimize the total error [122].

$$(Eq1)\ \ x[1] * \left(sin(2 * \pi * T + x[2])\right) + \ x[3] * (sin\left(2 * \pi * \frac{T}{2} + x[4]\right)) + \ x[5]$$

We then performed a Monte Carlo procedure on the fitted amplitude to evaluate whether the fitted data was modulated periodically as a function of the phase. 50,000 surrogates were generated for each participant, target position and frequency, by randomly assigning correct responses, i.e., for each target, we randomly assigned an incorrect or a correct response based on the averaged performance, and false alarms, i.e., a number of false alarms at an associated random delay was randomly assigned to each block, based on the average number of false alarms throughout the experiment. Hit and false alarm rates were then computed for each phase bin, position, and frequency, and fitted to the same sine function (Eq1). The surrogate distributions of the 50,000 fitted amplitudes for the induced frequency and its first harmonic separately were compared to the empirical fitted amplitudes. P-values were obtained by computing the proportion of fitted amplitudes equal or higher than the empirical fitted amplitude (fitted amplitudes: free parameters $x[1]$ and $x[3]$ from (Eq1)). Two participants were excluded from the analysis at this point because no significant phase effect was observed in the hit rates at position 1 in the 4-Hz condition (Bonferroni correction for multiple comparisons, i.e., the three positions; p-value threshold of 0.01). The reasoning for selecting this exclusion criterium is that a slow 4-Hz stimulation should induce a large effect in behavior [28, 123, 124], and such an effect should be the strongest the closest from the inducer. Note that false alarms were low in each phase bins (< 0.5%) and not significantly modulated periodically (except for the induced frequency 8 Hz, at position 1, $p < 0.01$; the p-value for the others induced frequencies and positions were not significant: Bonferroni correction across frequencies and positions, p-value threshold < 0.01, corresponding to a Z-score threshold of 2.64, and a Cohen's d threshold of 1.86). Consequently, in the next steps of the analysis, only hit rates were considered.

A group level analysis was also performed. Empirical and surrogate data were averaged across participants, and the same Monte Carlo procedure as presented above was performed. Bonferroni (p-value threshold < 0.01) was used to correct for multiple comparisons.

Variance explained by the spatial organization of targets. We hypothesized that the spatial organization of brain oscillations should explain a larger variance in the behavioral phase effect. To test this hypothesis, the hit rate was computed for each frequency and phase bin, regardless of target position. The hit rate was then fitted to the complex sine function (Eq1) and the amplitude modulation, i.e., difference in hit rate between the optimal and the non-optimal phase, was computed for each frequency and participant. Two-tailed t-tests were used to assess whether the amplitude modulation averaged across the three target positions was significantly different than the amplitude modulation computed across targets independently of their position, for each frequency.

Optimal phase shift between target positions for each induced brain oscillation. The optimal phase, i.e., the position on the fitted curve at maximal performance, was extracted for each target position and frequency, on data averaged across participants. We asked whether the optimal phase shift as a function of target positions was different between the four induced frequency conditions, i.e., whether there is a significant interaction between frequency and target position. We used a linear mixed effect model [125] to test for such an interaction.

We first computed phase-locking values for each optimal phase. The phase-locking value is obtained by dividing complex vectors, i.e., amplitude and phase information, by their length (i.e., amplitude), thus normalizing for amplitude and keeping only the phase, and then, computing the mean across the normalized vectors [126, 127]. Thus, to convert our measure of optimal phase in phase-locking values: 1) We created a distribution of optimal phases. The distribution was obtained with a bootstrap procedure. We generated 1,000 surrogate datasets by randomly selecting trials with an equal probability sampling from the initial datasets, and computing the optimal phase from each surrogate dataset, for each participant, frequency, and target position. 2) We converted the obtained optimal phases into complex vectors. The phase-

locking values were fitted to a linear mixed effects model with frequencies and target positions as fixed effects, and participants as random effect. Post-hoc tests allowed to assess which specific frequencies displayed a shift in the optimal phase. Here, the optimal phases were converted in radians. We created a one-cycle sine wave with the phase offset of the oscillating disk and extracted the phase values in radians along the entire cycle. We were then able to do a correspondence between the optimal phase extracted from data fitting, and the phase values in radians extracted from this one-cycle sine wave fit. Note that the same procedure was applied participant-by-participant to obtain rose plots of the individual optimal phase with the function circ_plot from the Circular Statistics Toolbox ([128], P. Berens, CircStat: A Matlab Toolbox for Circular Statistics, Journal of Statistical Software, Volume 31, Issue 10, 2009, http://www.jstatsoft.org/v31/i10), for each frequency and target position. The optimal phase in radians was compared between target positions by computing the pairwise phase difference with the function circ_dist from the Circular Statistics Toolbox. Statistics were performed with a Monte Carlo procedure. 50 000 datasets were created for each target position and frequency, by randomly assigning detection performance according to the average values for each pair of positions (positions 1 and 2, 1 and 3, 2 and 3), and by considering the original distribution of the number of targets across participants and phase bins. The data were fitted to the sine function (Eq1). The optimal phase was computed and converted in radians, and the phase difference was obtained for each pair of position. Thus, we obtained a surrogate of 50 000 phase differences for each pair of positions and each frequency. By computing the proportion of surrogate phase difference equal or higher than the real phase difference, we obtained p-values, FDR corrected for multiple comparisons across target positions and frequencies (p-value threshold of 0.01).

Supplemental Information

Supplemental Figure

The amplitude modulation, i.e., difference in hit rate between the optimal and the non-optimal phase, was computed on data averaged across participants, for each frequency and target position. A two-way repeated-measures ANOVA revealed a significant main effect of the frequency ($F(3, 42) = 31.48$, SS = 0.77, p-value < 0.01, $eta^2 = 69.22$), and no main effect of the target position ($F(2, 28) = 1.10$, SS = 0.01, p-value = 0.34, $eta^2 = 7.29$), nor of the interaction ($F(6, 84) = 0.73$, SS = 0.02, p-value = 0.62). The amplitude modulation was of 53.16 ± 2.91 % for 4 Hz, 49.04 ± 3.55 % for 6 Hz, 40.24 ± 2.84 % for 8 Hz, and 36.87 ± 2.59 % for 10 Hz (**Figure S1**). Post-hoc two-tailed t-tests showed that the amplitude modulation was higher for 4 Hz compared to 6 Hz (p-value = 0.03, Cohen's d = 0.32, CI = [0.01; 0.07]), 8 Hz (p-value < 0.01, Cohen's d = 1.16, CI = [0.09; 0.16]) and 10 Hz (p-value < 0.01, Cohen's d = 1.52, CI = [0.12; 0.20]), for 6 Hz compared to 8 Hz (p-value < 0.01, Cohen's d = 0.70, CI = [0.05; 0.12]) and 10 Hz (p-value < 0.01, Cohen's d = 1.01, CI = [0.08; 0.15]), and higher for 8 Hz compared to 10 Hz (p-value = 0.05, Cohen's d = 0.32, CI = [0; 0.06]). In summary, the amplitude modulation decreases with increasing frequency but is constant across target positions.

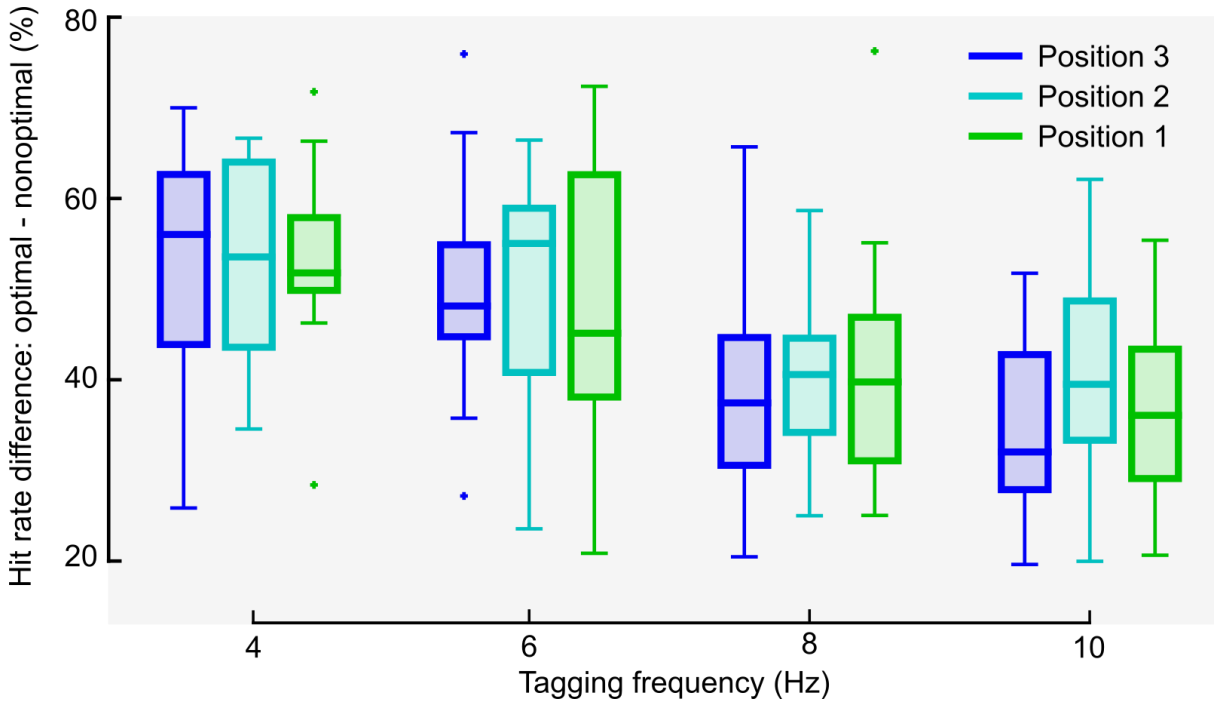

Figure S1. The amplitude modulation decreased with increasing induced frequency. *Amplitude computed as the difference between the maximum and the minimum hit rate. Dots, individual outlier data. A two-way repeated-measures ANOVA revealed a significant main effect of frequency ($F(3, 42) = 31.48$, SS = 0.77, p-value < 0.01, $eta^2 = 69.22$).*

Control experiment

Procedure

The targets were of same size and location as in the main experiment. The peripheral disk was, however, not modulated sinusoidally but was flashed (during three frames, for a total of 6.3 ms) at 7 different levels of luminance (7 contrast levels: 5%, 20.8%, 36.7%, 52.5%, 68.3%, 84.2% and 100%) at the same time as target onset to test for luminance masking. There was 20% of catch trials in which the disk was flashed but not the target.

As for the main experiment, the control experiment first included a staircase procedure to adjust the contrast of each target, for each participant, to reach 50% detection. In 7 blocks, the luminance of the disk was set at 50% contrast. For each block, 6 to 18 targets were presented (~10 targets/trials per block on average), thus the staircase procedure contained an average of 70 trials.

Then, participants performed four runs of 38 blocks each in two separate experimental sessions of approximately 1h30 each (no EEG recording for this control experiment). Each contrast level was displayed the same number of times (~217 targets per contrast level). Target contrasts were adjusted every 15 blocks to maintain the same detection level across the entire session.

Analyses

47.5 ± 56.4 targets were rejected from the analysis due to blinks or saccade eye movements. Hit rates, i.e., percentage of correct detection, median reaction times and target contrasts were computed for each target position. Hit rates were 57.18 ± 1.1 %, 51.74 ± 0.35 %, and 45.82 ± 0.76 % for position 1, 2 and 3, respectively. Median reaction times were 474 ± 2 ms, 511 ± 3 ms, and 525 ± 3 ms, for position 1, 2, and 3, respectively. Target contrasts were 0.61 ± 0.01 %, 1.16 ± 0.04 %, and 0.71 ± 0.02 %, for position 1, 2, and 3, respectively. A one-way repeated-measures ANOVA was performed for each dependent variable to assess the effect of target position. For hit rates, there was no main effect of target position ($F(1,14) = 2.52$, p-value = 0.09, $eta^2 = 15.29$). For median reaction times, there was also no main effect of target position ($F(1,14) = 1.24$, p-value = 0.30, $eta^2 = 8.16$). The absence of a significant main effect of target positions in any of these two tests confirm successful contrast manipulation. For target contrast, there was a main effect of target position ($F(1,14) = 13.68$, p-value < 0.01, $eta^2 = 49.42$), which is coherent with the staircase manipulation.

Targets were binned according to the level of luminance of the simultaneously presented disk. To emulate an oscillatory cycle (which, in the main experiment, goes from 0% contrast to 100% and back to 0%), we used a bootstrap procedure (5 000 repetitions) randomly assigning half of the targets to one half of the cycle (from contrast 0% to 100%), while the other half was assigned to the second half of the cycle (from contrast 100% to 0%), thus resulting in 13 luminance levels.

The number of false alarms (i.e., participants responded a target was present while it was absent), and the number of hits were computed for each target position and for the 13 luminance levels. Individual data and data averaged across participants were fit to a one-cycle sine function (EqS1) with the following free parameters: the amplitude, $x[1]$, the phase offset, $x[2]$, the baseline, $x[3]$. To find the parameters that best fit the data, we used a Least Squares cost function, i.e., the cost function computed the total squared errors, i.e., the sum of squared error, between the fit and the data, giving a measure of how well the data are fitted. The best fit is the one whose parameters minimize the total error [122].

$$(EqS1)\ \ (x[1] * \big(sin(2 * \pi * T + x[2])\big) + \ x[3]$$

We performed a Monte Carlo procedure on the fitted amplitudes to assess whether the fitted data was modulated periodically by the luminance disk. 50 000 surrogates were generated for each participant by randomly assigning detection performance based on the average performance at each contrast and position (as for the empirical data, an oscillatory cycle was emulated using a bootstrap procedure). The surrogate data was fit to the one-cycle sine function (EqS1). The empirical averaged data was compared

to the averaged surrogate distribution by computing the proportion of fitted amplitudes equal or higher than the empirical fitted amplitude. P-values were corrected for multiple comparisons using Bonferroni correction (p-value threshold of 0.01). There was no significant effect of luminance, at any target position, for the false alarm ratio and thus we did not consider this variable any further.

The optimal phase, i.e., phase of highest performance, was computed for each target position on data averaged across participants. To study whether the optimal phase shifted as a function of target positions, we computed the pairwise phase difference and assessed the significance using a Monte Carlo procedure. 50 000 datasets were created for each target position by randomly assigning detection performance according to the average values for each pair of positions (positions 1 and 2, 1 and 3, 2 and 3), and by considering the original distribution of the number of targets across participants and luminance values. The data were fitted to the sine function (EqS1) and the pairwise phase difference was obtained for each pair of positions. We obtained a surrogate of 50 000 phase differences for each pair of positions. P-values were obtained by computing the proportion of surrogate phase differences equal or higher than the empirical phase difference.

Results

To assess whether the periodicity observed in behavioral data was due to luminance masking from the disk, 15 participants performed the above-mentioned control experiment. Detection performance showed a significant oscillatory pattern at each target position (Monte Carlo, Bonferroni corrected across positions, p-value threshold of 0.01, corresponding to a Z-score threshold of 2.12, and a Cohen's d threshold of 1.31, **Figure S2A**).

Seven participants took part in both the main and the control experiment. For these participants, we overlapped in **Figure S2B-H** the sine fits from the control experiment and for the 10 Hz induced frequency from the main experiment. The oscillatory patterns clearly differed between the two experiments. Crucially, unlike in the main experiment, in the control experiment no phase shift between positions was found (p-value = 1, i.e., the pairwise phase differences were the same between the empirical and surrogate datasets).

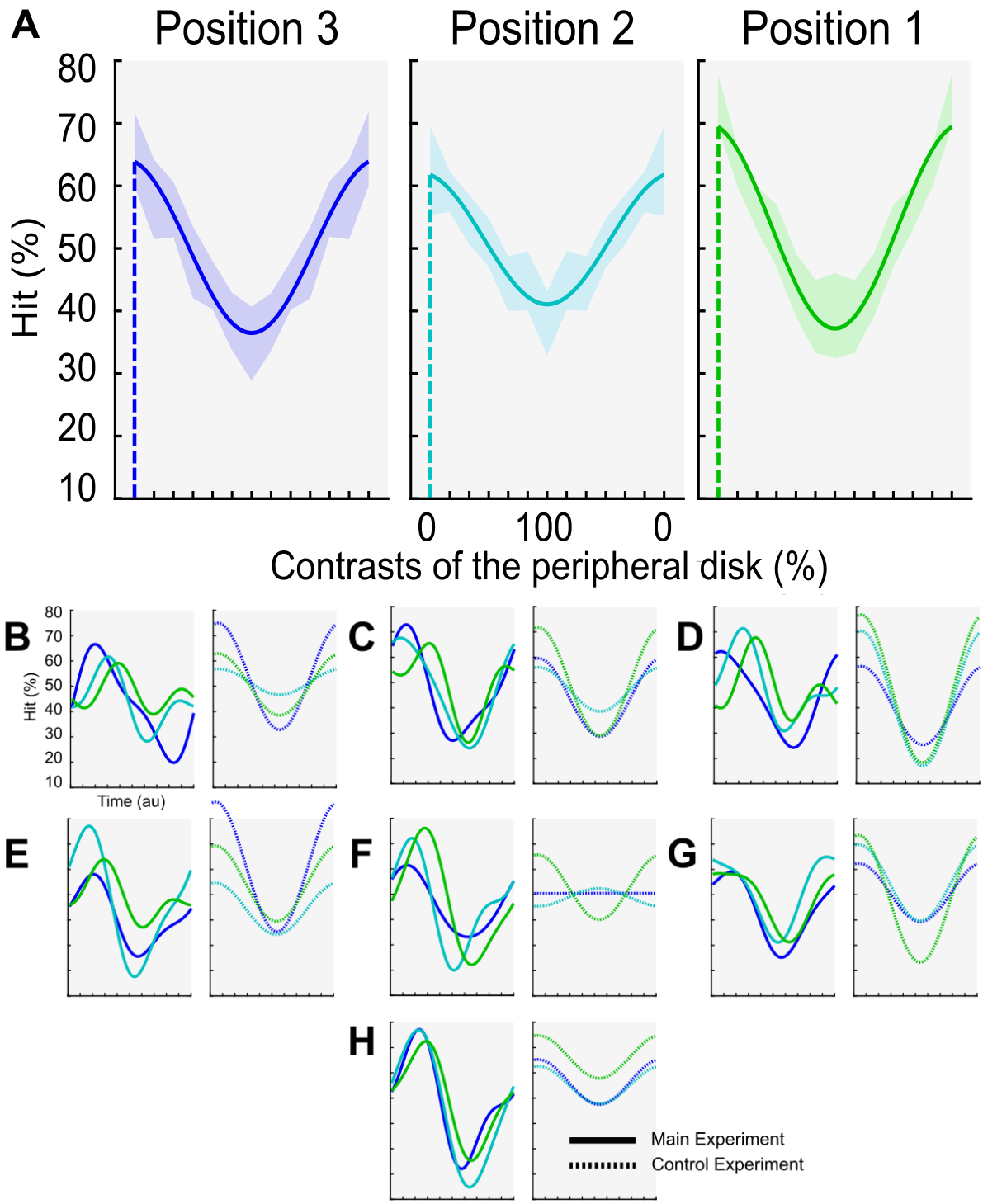

Figure S2. The propagation of perceptual cycles was not due to luminance masking. A. *Hit rate for each 13 luminance levels and the 3 target positions averaged across participants (n=15) and fitted to a one-cycle sine function. Shaded colored area, 95 confidence intervals. Solid line, fit. Dotted line, optimal phase.* ***B – H*** *Results from individual participants for the main experiment on the left and the control Experiment on the right. Green, position 1. Cyan, position 2. Blue, position 3.*